Pirou, S.; García-Fayos, J.; Balaguer Ramirez, M.; Kiebach, R.; Serra Alfaro, JM. (2019). Improving the performance of oxygen transport membranes in simulated oxy-fuel power plant conditions by catalytic surface enhancement. Journal of Membrane Science. 580:307-315. https://doi.org/10.1016/j.memsci.2019.03.027

Improving the performance of oxygen transport membranes in simulated oxy-fuel power plant conditions by catalytic surface enhancement

Stéven Pirou[a*], *Julio García-Fayos*[b], *María Balaguer*[b], *Ragnar Kiebach*[a], *José M. Serra*[b]

[a] Department of Energy Conversion and Storage, Technical University of Denmark, Risø campus, Frederiksborgvej 399, DK-4000 Roskilde, Denmark

[b] Instituto de Tecnología Química (Universitat Politècnica de València – Consejo Superior de Investigaciones Científicas), Av. Naranjos s/n, E-46022 Valencia, Spain

E-Mail addresses: stepir@dtu.dk, jugarfa@itq.upv.es, mabara@upvnet.upv.es, woki@dtu.dk, jmserra@itq.upv.es

[*] Corresponding author

Abstract

The stability of dual-phase oxygen transport membranes consisting of 70 vol.% $(Y_2O_3)_{0.01}(Sc_2O_3)_{0.10}(ZrO_2)_{0.89}$ and 30 vol.% $MnCo_2O_4$ (10Sc1YSZ-MCO (70-30 vol.%)) was investigated in simulated oxy-fuel power plant flue-gas (250 ppm SO_2, H_2O, balance CO_2). Additionally, the influence of catalytic porous backbones on the performance of the membrane was studied in the same conditions. The chemical stability of the dual-phase membrane was investigated by X-ray diffraction (XRD), Raman spectroscopy and scanning electron microscopy (SEM). The tests performed before and after the exposure to the simulated flue gas showed excellent chemical stability. Electrochemical impedance spectroscopy (EIS) measurements were performed on activated and non-activated porous catalytic backbones made of: (i) 8YSZ, (ii) 8YSZ-MCO (40-60 vol.%), (iii) 10Sc1YSZ-MCO (40-60 vol.%), (iv) 10Sc1YSZ-MCO (70-30 vol.%), and (v) $Ce_{0.8}Tb_{0.2}O_{2-\delta}$ (CTO) - $NiFe_2O_4$ (NFO) (40-60 vol.%) to achieve a better understanding of the oxygen surface reactions (especially in SO_2 and CO_2 containing atmospheres). The lowest polarization resistances (R_p) were found for 10Sc1YSZ-MCO (40-60 vol.%) and CTO-NFO (40-60 vol.%) porous backbones. Oxygen permeation tests realized on 10Sc1YSZ-MCO membranes demonstrated that the catalytic porous backbones can significantly influence the oxygen permeation flux, and improvements of up to 55 % were achieved. Both EIS and oxygen permeation measurements showed a significant influence of SO_2 on the oxygen oxidation/reduction reactions (increase of R_p, decrease of oxygen permeation fluxes) due to SO_2 adsorption and blocking of active sites for the oxygen reactions. Nevertheless, no microstructural degradation was found after SO_2 exposure and initial R_p values and oxygen permeation fluxes could be recovered in most cases.

Keywords

Oxygen transport membrane, Dual-phase membrane, Catalytic backbone, SO_2 stability, Oxy-fuel combustion, carbon capture

Highlights

- 10Sc1YSZ-MCO membranes are stable under oxy-fuel relevant conditions.
- A catalytic porous backbone on the membrane improves the efficiency to transport oxygen.
- Oxygen fluxes-up to 0.28 $mL_N\ cm^{-2}\ min^{-1}$ (850 °C, air/Ar) measured.

1. Introduction

The reduction of CO_2 emissions is currently an important challenge for the society. This mission can be achieved by introducing gas separation techniques to capture and store CO_2 from large point sources like fossil fuel power plants, steel plants or cement kilns. Among the available technologies for Carbon Capture and Storage (CCS), oxy-fuel combustion is a promising option. This approach uses pure oxygen to combust the fossil fuel, resulting in flue-gases consisting mainly of CO_2 (90-95 %) and steam [1][2]. Typically, cryogenic air separation units (ASUs) are used to produce the required oxygen. While this technique is mature, the process is particularly expensive and consumes a considerable amount of energy [3][4]. Ceramic oxygen transport membranes (OTMs) that supply the oxygen needed for the combustion process may, when thermally integrated, operate more efficiently, using less energy [5][6][7].

OTMs are typically formed by Mixed Ionic Electronic Conductors (MIEC), which allow oxygen diffusion through vacancies in the crystal lattice and simultaneous transport of electrons in the opposite direction. The membranes are fully dense which results in a high selectivity in the separation. An oxygen partial pressure differential between an oxidizing gas (air at 0.21 atm) and a reducing gas (recirculated flue gas at $pO_2 \approx 10^{-2}$ atm [8]) exists across the membrane, providing a driving force for the oxygen separation allowing oxygen ion transport from the high oxygen partial pressure side to the low oxygen partial pressure side. Membranes based on single MIEC materials can achieve high oxygen fluxes [9][10][11][12][13][14][15][16][17][18][19], however most of the promising materials are not chemically stable under atmosphere containing CO_2 and SO_2 [12][20][21][22][23][24][25][26], which is particularly required for oxy-fuel combustion applications. Dual-phase composites consisting of separated ionic and electronic conductor phases are a promising alternative approach to ensure high oxygen flux and chemical stability in realistic power plant conditions.

Dual-phase membranes consisting of a thin (7 μm) dense layer made of 70 vol.% of $(Y_2O_3)_{0.01}(Sc_2O_3)_{0.10}(ZrO_2)_{0.89}$ (10Sc1YSZ) as ionic conductor and 30 vol.% of $MnCo_2O_4$ (MCO) as electronic conductor, supported on a $(Y_2O_3)_{0.03}(ZrO_2)_{0.97}$ (3YSZ) porous support, were developed and tested in a previous study [27]. The study showed

the excellent stability of the asymmetric membrane in CO_2 containing atmosphere and oxygen permeation fluxes as high as 1.41 $ml_N\ min^{-1}\ cm^{-2}$ and 2.23 $ml_N\ min^{-1}\ cm^{-2}$ were obtained at 940 ºC in air/N_2 and O_2/N_2 atmospheres, respectively.

Assuming that the oxygen flux produced by the membrane is in direct proportion with its thickness, thin asymmetric membranes are advantageous to minimize the resistance arising from bulk diffusion. In this case, other mechanisms such as catalytic surface exchange and gaseous transport become limiting factors of the oxygen separation as reported in literature [27]. Consequently, further improvement of the catalytic activity at the surface is required. In order to enhance the surface exchange kinetics, electro-catalytic materials (referred as *catalytic porous backbones* throughout this study) can be applied on both sides of the membrane [28].

The present article studies the stability of 10Sc1YSZ-MCO dual-phase membranes and the influence of catalytic porous backbones on the oxygen permeation under conditions relevant for oxy-fuel combustion. The stability of a 7 µm thick asymmetric membrane was evaluated by a 170 h long test performed in simulated oxy-fuel power plant flue-gas (250 ppm SO_2 + 5 % O_2 + 3 % H_2O balanced in CO_2 [8]). Several characterization techniques (X-ray diffraction (XRD), Raman spectroscopy and scanning electron microscopy (SEM)) were used to verify the possible utilization of the membrane for direct application in oxy-fuel power plants. To further improve the membrane performance, five catalytic porous backbone materials; (i) $(Y_2O_3)_{0.08}(ZrO_2)_{0.92}$ (8YSZ), (ii) 8YSZ-MCO (40-60 vol.%), (iii) 10Sc1YSZ-MCO (40-60 vol.%), (iv) 10Sc1YSZ-MCO (70-30 vol.%), and (v) $Ce_{0.8}Tb_{0.2}O_{2-\delta}$ (CTO)-$NiFe_2O_4$ (NFO) (40-60 vol.%) were prepared, and characterized by electrochemical impedance spectroscopy (EIS). The impact of the catalytic activation of the backbones (infiltration of electro-catalytic solutions) on the efficiency of the oxygen separation was investigated and the oxygen permeation was measured in simulated oxy-fuel conditions (sweep gas: CO_2 + SO_2 + Ar).

2. Experimental

2.1. Preparation of porous backbones

Five screen-printable inks made of (i) 8YSZ, (ii) 8YSZ-MCO (40-60 vol.%), (iii) 10Sc1YSZ-MCO (40-60 vol.%), (iv) 10Sc1YSZ-MCO (70-30 vol.%), and (v) CTO-NFO (40-60 vol.%) were prepared by milling the powders with a 6 wt.% ethylcellulose-terpineol solution in a 1:1 weight ratio by using a triple roll mill. The 8YSZ powder used to prepare the ink (i) was purchased from Tosoh (Japan). The composite powders (ii), (iii), and (iv) were prepared by milling 8YSZ (Tosoh, Japan), MCO (Marion Technologies, France) and 10Sc1YSZ (Daiichi Kigenso Kagaku Kogyo Co. Ltd, Japan) commercial powders in ethanol using zirconia balls for 24 h. CTO-NFO (40-60 vol.%) was prepared by one pot Pechini method as described by Garcia-Fayos *et al.* in a previous study [29].

2.2. Membranes fabrication

Thin (7 μm) asymmetric supported membranes made of 70 vol.% of 10Sc1YSZ and 30 vol.% of MCO were prepared to study the thermochemical stability of the membrane under oxy-fuel power plants conditions. More robust membranes of 0.5 mm thick able to support higher pressure were required for oxygen permeation tests. This section describes the fabrication processes of these two membrane architectures.

2.2.1. Thick symmetric membrane

The ionic (10Sc1YSZ, Daiichi Kigenso Kagaku Kogyo Co. Ltd, Japan) and electronic ($MnCo_2O_4$, Marion Technologies, France) conductors were blended in a 70-30 vol.% ratio to form the 10Sc1YSZ-MCO composite material. The particle size of the powders was adjusted to the submicron range by 24 h of ball-milling in ethanol. After drying, the composite powder was uniaxially pressed on a 26 mm diameter steel die (50 MPa) to form green disks. The disks were sintered at 1250 ºC for 6 h in air, and afterwards polished down to 0.5 mm by using SiC polishing papers. In-house made inks of (i) 8YSZ, (ii) 10Sc1YSZ-MCO (70-30 vol.%) and (iii) CTO-NFO (40-60 vol.%) were screen-printed on both sides of the membranes to serve as catalytic porous backbones. However, one of the membrane was kept without backbone coatings. To obtain similar porosity for all catalytic porous backbones and therefore be able to compare their performances while neglecting the gas diffusion parameter, the coated membranes were calcined at different temperatures and the porosity of the backbones was checked by SEM. Thus,

the 8YSZ porous backbone was formed at 1150 ºC, CTO-NFO at 1100ºC, while 10Sc1YSZ-MCO were treated at 975 ºC (2 h in air). To overcome slow surface exchange/reaction kinetics, the backbones were infiltrated by a 2 M precursor solution of Ce-Pr catalyst (molar ratio 1:1) prepared by dilution of Ce and Pr nitrates in ethanol/water. Figure 1 presents schematic illustrations of the thick symmetrical membranes tested.

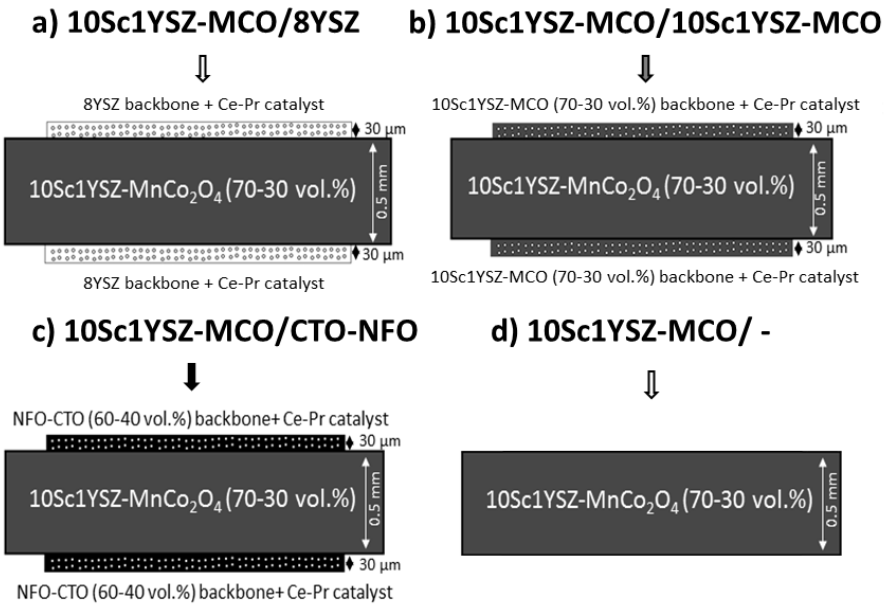

Figure 1: Schematic illustrations of the 0.5 mm thick 10Sc1YSZ-MCO symmetrical membranes prepared for oxygen permeation measurements. Each membrane was coated with a different backbone material: a) 8YSZ, b) 10Sc1YSZ-MCO, c) CTO-NFO and d) no coatings.

2.2.2. Thin asymmetric membrane

As presented Figure 2, the asymmetric membrane consists of a three distinct layers: a 300 µm thick porous support (3YSZ + 20 vol.% of Al_2O_3), a 10 µm thick porous 8YSZ inter-layer and a thin (7 µm) 10Sc1YSZ-MCO dense layer (post-sintering thicknesses). All layers were manufactured separately by tape-casting. Then, the green tapes were assembled by lamination at 135 °C and disks were cut out using a stamping tool. A two-step sintering including a peak temperature at 1225 °C (3 min) and a dwell temperature of 1090 °C (6 h) was used to develop the asymmetric membranes. The complete manufacturing procedure of the 10Sc1YS-MCO asymmetric membranes was detailed in a previous study [27].

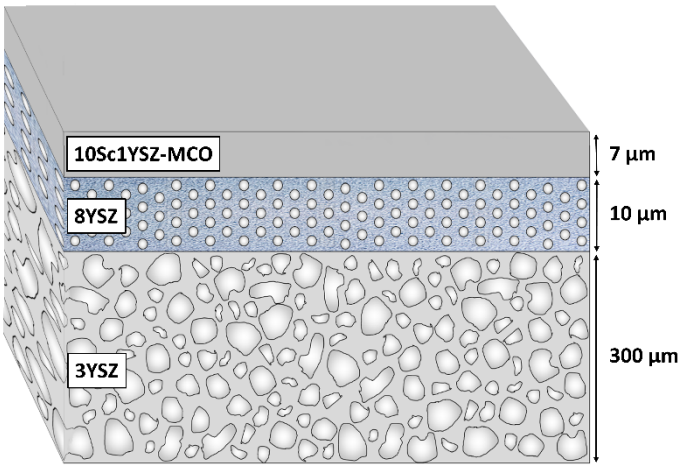

Figure 2: Schematic illustration of the thin asymmetric 10Sc1YSZ-MCO membrane used for the long-term stability test in oxy-fuel conditions.

2.3. Characterization

2.3.1. Thermochemical stability test and material characterization

The thermochemical stability of a 7 µm thin asymmetric membrane was studied in a quartz horizontal testing unit. The testing unit was installed in an oven and heated up to 850 ºC in wet N_2 (3 % H_2O). When the temperature was reached, the gas composition was switched to a gaseous mixture containing 250 ppm of SO_2 and 5 % of O_2 balanced in CO_2. The gaseous mixture was provided by a pre-mixed gas cylinder (Linde). Wet gas conditions (3 % H_2O) were supplied by bubbling the gas stream through water at room temperature. The asymmetric membrane was in direct contact with the gas mixture flowing at 10 ml_N min^{-1} for 170 h. After the exposure of the membrane to the gas atmosphere, the testing unit was cooled down in wet N_2 by natural convection (20-25 °C min^{-1}).

To compare the microstructure of the tested asymmetric membrane with a similar untested membrane, X-ray diffraction (XRD), Raman spectroscopy and scanning electron microscopy with energy-dispersive X-ray spectroscopy (SEM-EDX) analyses were performed.

The XRD measurements were carried out using a PANalytical Cubix fast diffractometer, using CuKα1 radiation (λ = 1.5406 Å) and a X'Celerator detector in Bragg−Brentano geometry. XRD patterns recorded in the 2θ range from 10° to 90° were analyzed using X'Pert Highscore Plus software.

SEM-EDX analyses were performed using a ZEISS Ultra55 field emission scanning electron microscope.

Raman spectra were measured with a Renishaw inVia Raman spectrometer equipped with a Leica DMLM microscope and a 514-nm Ar+ ion laser as an excitation source. A x50 objective of 8-mm optical length was used to focus the depolarized laser beam on a spot of about 3 μm in diameter. The Raman scattering was collected with a charged coupled device (CCD) array detector.

2.3.2. Electrochemical Impedance Spectroscopy

Electrochemical Impedance Spectroscopy (EIS) measurements were performed on 1 mm thick fully dense $Ce_{0.8}Gd_{0.2}O_{2-\delta}$ (GDC) electrolytes sintered at X ºC for Y h and coated on both sides by the studied backbone materials: (i) 8YSZ, (ii) 8YSZ-MCO (40-60 vol.%), (iii) 10Sc1YSZ-MCO (40-60 vol.%), (iv) 10Sc1YSZ-MCO (70-30 vol.%), and (v) CTO-NFO (40-60 vol.%). As stated in the section 2.2.1., to obtain similar porosity for all catalytic layers the coated GDC electrolytes were calcined at different temperatures. The performance of the backbones was investigated with and without infiltrations of a homemade catalytic solution of Ce and Pr nitrates (excepting 8YSZ, only tested with catalyst infiltrations because it is a purely ionic conductor). The catalyst infiltration was identically processed for all backbones. The infiltrated backbones were treated at 850 ºC for 2 h in air. Finally, a top gold mesh was painted on the surfaces of all samples in order to ensure proper current collection during the EIS measurements.

The symmetrical cells were tested by means of electrochemical impedance spectroscopy in a two-point configuration. Input signal was 0 V DC – 20 mV AC amplitude in the $0.01 – 3 \cdot 10^5$ Hz frequency range. This signal was generated by a Solartron 1470E and a 1455A FRA module equipment. EIS measurements were performed at 850 ºC, under several atmospheres ((i) 21 % O_2 in N_2, (ii) 5 % O_2 in N_2, (iii) 5 % O_2 in CO_2 and (iv) 250 ppm SO_2

+ 5 % O_2 in CO_2). In all cases, the total gas flow remained constant (100 ml·min^{-1}). Zview™ 2 fitting programme was employed to analyze the impedance spectra.

2.3.3. Oxygen permeation tests

Oxygen permeation tests were carried out in a lab-scale quartz reactor (Figure 3). Synthetic air (21 %, vol. O_2) was fed with a flow rate of 100 mL_N min^{-1}, while argon, CO_2 and SO_2 mixtures were used as sweep gases on the permeate side in a 4-end mode configuration with a flow rate of 150 mL_N min^{-1}. The flow rates were controlled by mass flow controllers. Both streams were fed at atmospheric pressure. The temperature was measured by a thermocouple attached to the membrane. A PID controller maintained the temperature within 2 ºC of the set point. Gas-tight sealing was achieved using O-rings with tailored alloys for sealing at 850 ºC. The permeate was analyzed at steady state by online gas chromatography using a micro-GC Varian CP-4900 equipped with Molsieve5A, Pora-Plot-Q glass capillary, and CP-Sil modules. Oxygen concentration was calculated from the O_2 signal area and its response factor previously calibrated. The total oxygen permeation was calculated as the product of the O_2 concentration ($\%O_{2,permeate}$) and the sweep flow ($\dot{n}''$). The oxygen permeation flux (J_{O_2}) was then determined from the division of the total oxygen permeation by the effective area (A) of the membrane as:

$$J_{O_2} = \%O_{2,permeate} \cdot \frac{\dot{n}''}{A} \qquad (1)$$

To ensure leak free conditions the nitrogen concentration in the permeate gas was continuously controlled. Oxygen related to minor leaks was removed from J_{O_2} calculation by taking into account the presence of N_2 in the permeate stream. Therefore, the permeating oxygen ($\%O_{2,permeate}$) was calculated as:

$$\%O_{2,permeate} = \%O_{2,GC} - \left(\frac{0.21}{0.79} \cdot \%N_{2,GC}\right) \qquad (2)$$

where $\%O_{2,GC}$ and $\%N_{2,GC}$ are the percentages of oxygen and nitrogen measured by the gas chromatography in the permeate, respectively.

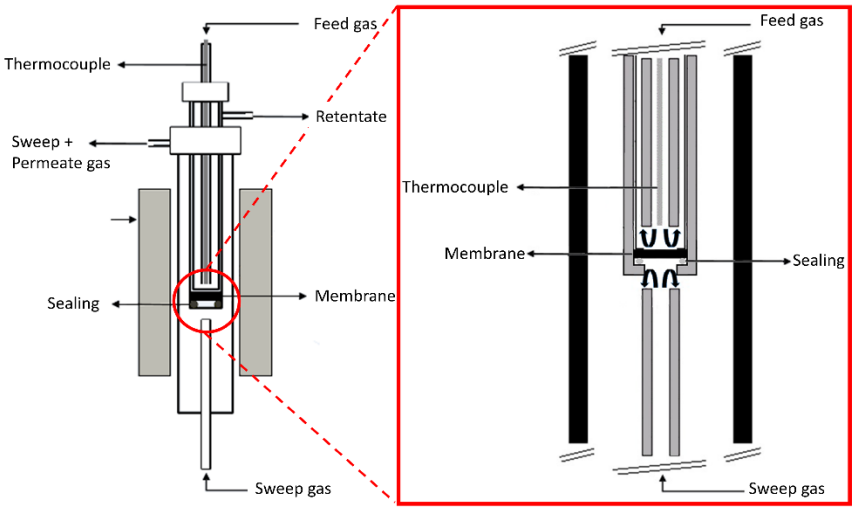

Figure 3: Schematic illustration of the lab-scale quartz reactor used for the oxygen permeation tests.

3. Results and discussion

3.1. Thermochemical stability in oxy-fuel conditions

To investigate the applicability of the membrane in oxy-fuel power plants, the effects on the membrane of a gas stream containing CO_2, SO_2 and H_2O were studied.

In this section, post mortem analyses (XRD, Raman spectroscopy and SEM) of a membrane exposed to a continuous flow of simulated oxy-fuel power plant flue-gas (250 ppm of SO_2, 5 % of O_2, 3 % of H_2O balanced with CO_2) during 170 h at 850 ˚C are presented and compared to an untested sample.

Figure 4 shows the XRD diffractograms of the treated and untreated 10Sc1YSZ-MCO membranes. Both diffractograms are comparable, additional diffraction peaks related to the formation of new crystalline phases could not be observed, and all observed peaks belong to 10Sc1YSZ [30][31][32] or $MnCo_2O_4$ (JCPDS card No. 23-1237).

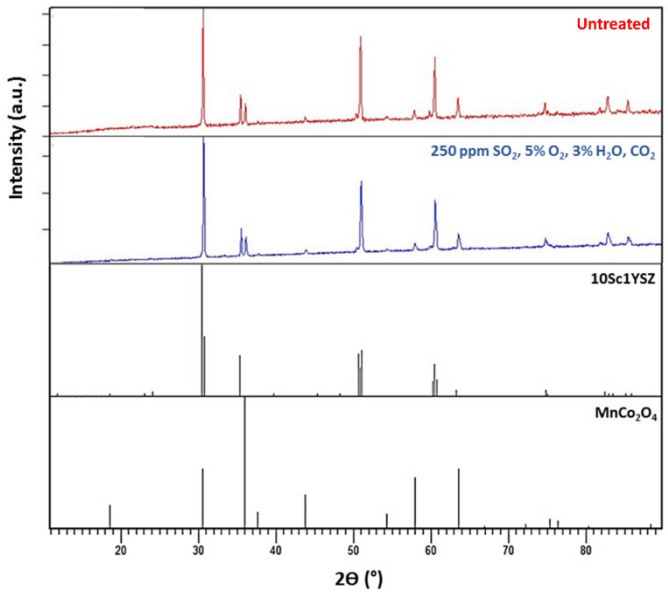

Figure 4: XRD diffractograms of treated and untreated 10Sc1YSZ-MCO membranes and XRD patterns of 10Sc1YSZ and $MnCo_2O_4$.

Knowing that it is difficult/not possible to detect very low amounts of crystalline phases or non-crystalline phases with XRD analysis, additional Raman spectroscopy was performed (Figure 5). This technique is well suited for the detection of small amount of carbonates or sulfates, however no additional peaks were found in the spectra of the treated membrane, suggesting that the exposure to the different gases did not create any new phases.

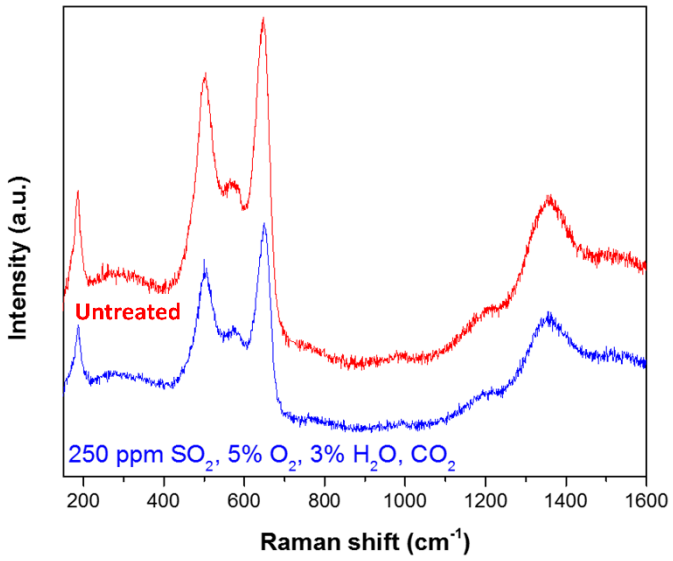

Figure 5: Raman spectra of treated and untreated 10Sc1YSZ-MCO membranes.

Figure 6 shows SEM images of the cross-sections of treated and untreated membranes. No evidence of interface reactions or cracks in the dense membrane layer during the long-term exposure was found. The 10Sc1YSZ-MCO layer remains fully dense and well attached to the porous supporting layers. Neither carbon nor sulfur were detected by EDX analysis, thus discarding the presence of carbonates or sulfates in the treated membrane.

Overall, the combined analyses confirmed the stability of the composite material and the membrane assembly at 850 °C under conditions relevant for oxy-fuel combustion.

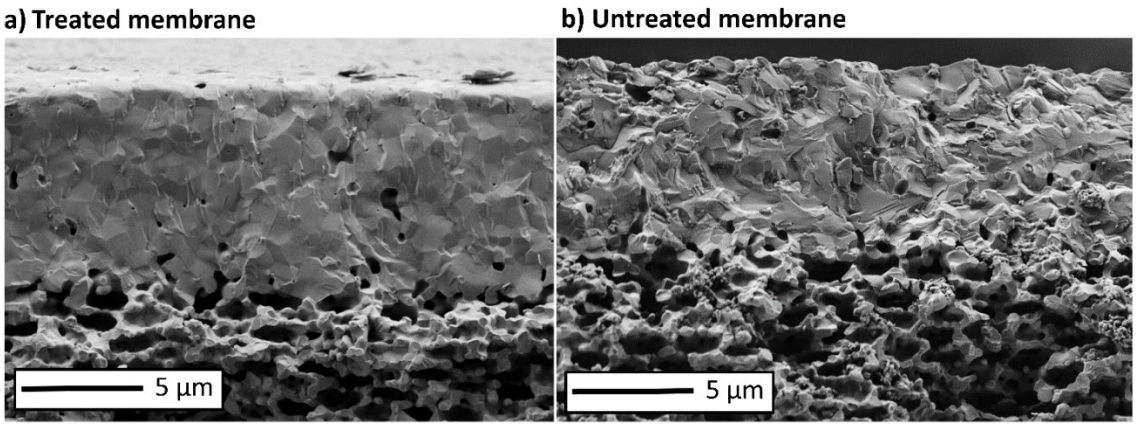

Figure 6: SEM images of cross-sections of 10Sc1YSZ-MCO asymmetric membranes (a) exposed to a continuous flow of CO_2 with 250 ppm of SO_2, 5 % of O_2, and 3 % of H_2O during 170 h and (b) unexposed.

3.2. Characterization of catalytic porous backbones by electrochemical impedance spectroscopy

EIS measurements were performed on dense $Ce_{0.8}Gd_{0.2}O_{2-\delta}$ symmetrical cells and results were processed to obtain the resistances associated to the porous backbones. Only the contributions in the negative imaginary part were taken into account to calculate these resistances. The values were corrected by the area of the porous backbones and the resulting values were divided by two, since both surfaces of the cells were coated. The final numbers correspond to the polarization resistance (R_p) of the porous backbones. R_p can give an idea of the conductivity of every catalytic system (the lower the R_p, the higher the conductivity of the porous backbone). In this section the R_p of the different catalytic porous backbones are compared. The influence of the ionic conductivity, the electronic conductivity, the catalytic activation and the impurities (SO_2, CO_2 and H_2O) on the R_p are discussed.

Electrical and ionic conductivities of the relevant materials are summarized in Table 1.

Figure 7 and Figure 8 present the R_p of the porous backbones with and without catalyst infiltrations. Due to a lack of an electronic conducting phase, the 8YSZ porous backbones cannot efficiently catalyze the oxygen oxidation/reduction reactions. Consequently, cells coated with 8YSZ backbones were only tested with Ce-Pr catalyst infiltrations (Figure 8).

Table 1: Electrical and ionic conductivities of materials used to prepare the porous backbones.

	Material	Electrical conductivity (S cm^{-1}) in air	Ionic conductivity (S cm^{-1}) in air	Ref
Ionic conducting materials	$(Y_2O_3)_{0.08}(ZrO_2)_{0.92}$ (8YSZ)	-	0.030 (850 °C)	[33]
	$(Y_2O_3)_{0.01}(Sc_2O_3)_{0.10}(ZrO_2)_{0.89}$ (10Sc1YSZ)	-	0.072 (840 °C)	[34]
	$Ce_{0.8}Tb_{0.2}O_{2-\delta}$ (CTO)	-	0.035 (800 °C)	[35]
Electronic conducting materials	$MnCo_2O_4$ (MCO)	60 (800 °C)	-	[36]
	$NiFe_2O_4$ (NFO)	0.26 (800 °C)	-	[36]

3.2.1. Influence of ionic conductivity, electronic conductivity, and catalyst activation on polarization resistances

The influence of the ionic conductivity on the ability of the backbones to transport oxygen can be evaluated by comparing the R_p of 8YSZ-MCO (40-60 vol.%) and 10Sc1YSZ-MCO (40-60 vol.%) composites. Indeed, with 0.072 S cm^{-1} at 840˚C, [34] 10Sc1YSZ presents 2 times higher ionic conductivity than 8YSZ (0.030 S cm^{-1} at 850˚C [33]). The experiments showed that the ionic conductivity of the porous backbones significantly influences the R_p, especially when the backbones are not infiltrated. Thus, the 10Sc1YSZ-MCO (40-60 vol.%) porous backbone presents R_p values approximately 8 times lower than the 8YSZ-MCO (40-60 vol.%) porous backbone (Figure 7). Similar conclusions can be drawn for the activated porous backbones (Figure 8), even though the difference between the 8YSZ-MCO (40-60 vol.%) and the 10Sc1YSZ-MCO (40-60 vol.%) porous backbone is not as pronounced (2 times lower).

The influence of the electronic conductivity on the R_p can be noticed by varying the content of the electronic conducting phase in the composite. In this study, the ratio of ionic/electronic conductors of the 10Sc1YSZ-MCO composite was varied. The increase of MCO resulted in a significant decrease in R_p for both activated and non-

activated backbones. As expected, the highest R_p among the activated backbones was obtained for the 8YSZ backbone. The 10Sc1YSZ-MCO (70-30 vol.%) composite presents the second highest R_p of the tested backbones. As shown in the Bode plot (Figure 9.a), processes contributing to the high frequencies part of the spectra are mainly responsible for the large R_p value. These processes are related to the transport of species through the 10Sc1YSZ-MCO/Ce-doped material interface [37], which could indicate that a lack of electronic conductivity limits the performance of this backbone. When the content of the electronic conducting phase was increased from 30 % to 60 %, lower Z'' values were obtained (Figures 9.a and 9.b) resulting to 3 to 7 times lower R_p, underlining the conclusions drawn above.

The infiltration of nano-particulate Ce and Pr catalysts into the porous catalytic backbones increases the catalytic surface area for oxygen oxidation/reduction reactions and therefore improves the ability of the backbones to incorporate and transport oxygen. Consequently, in every studied atmospheres activated porous catalytic backbones present lower R_p than non-activated backbones. The largest improvement was observed for the two backbones having the lowest ionic conductivity (8YSZ-MCO (40-60 vol.%) and CTO-NFO (40-60 vol.%)), see ionic conductivities Table 1).

To resume, EIS measurements showed that the material serving as porous catalytic backbone should preferably have a good ionic conductivity and a good electronic conductivity. To illustrate this importance, Figure 10 presents the reaction mechanism of the oxygen reduction reaction (ORR) taking place in the porous catalytic backbone at the high P_{O2} side (feed side). Two cases are distinguished: (i) a membrane coated with a porous backbone made of a composite of a good ionic conductor and a good electronic conductor (e.g. 10Sc1YSZ-MCO, CTO-NFO) and (ii) a membrane coated with a porous backbone made of a single ionic conducting phase (e.g. 8YSZ). As described by the Equation 3, the ORR requires oxygen gas (O_2) and electrons (e^-) to form oxide ions (O^{2-}). Once the oxygen ions are formed, a percolating ionic conducting phase is required to lead them to the membrane and therefore allow the oxygen permeation. Consequently, a good mix of ionic and electronic conducting phases is beneficial to increase the number of triple phase boundary. Figure 10 illustrates the difference of area available for the ORR if

a mixed ionic and electronic conductive (MIEC) material or a purely ionic conductive material is used as porous catalytic backbone. For the MIEC material, the area for the ORR is extended along the entire surface of the backbone, while for a purely ionic conducting material only the interface of the porous backbone and the dense membrane layer is suitable for the reaction. The oxygen oxidation reaction (OOR) reforming the gas after the permeation of the oxide ions through the membrane requires also the triple phase boundary zones and could have been taken as an example in the same way that the ORR. In this sense, the composites having the most beneficial mixed of ionic and electronic conductivity (10Sc1YSZ-MCO (40-60 vol.%) and CTO-NFO (40-60 vol.%)) are therefore the two most suitable porous catalytic backbones among the tested candidates to transport oxygen.

Oxygen reduction reaction: $O_2 + 4e^- = 2O^{2-}$ (3)

3.2.2. Influence of oxy-fuel conditions on the polarization resistances

As described in section 2.3.2., EIS measurements were performed at 850 ºC under clean conditions and under oxy-fuel combustion conditions. A strong influence of SO_2 on the oxygen oxidation/reduction reactions was observed. As shown by Figure 9, SO_2 enlarges the magnitude of resistive processes appearing at low frequencies, probably due to SO_2 adsorption leading to the blocking of active sites for the oxygen reactions [29]. Depending on the materials, the R_p of activated backbones are 2.5 to 10 times larger in contact to SO_2 than in air, and 2.5 to 6 times larger for non-activated backbones. Nevertheless, the material structure of the backbones was not irreversibly altered upon sulfur exposure and most of the initial R_p values were recovered after a short time in clean atmosphere (5 % O_2 in N_2).

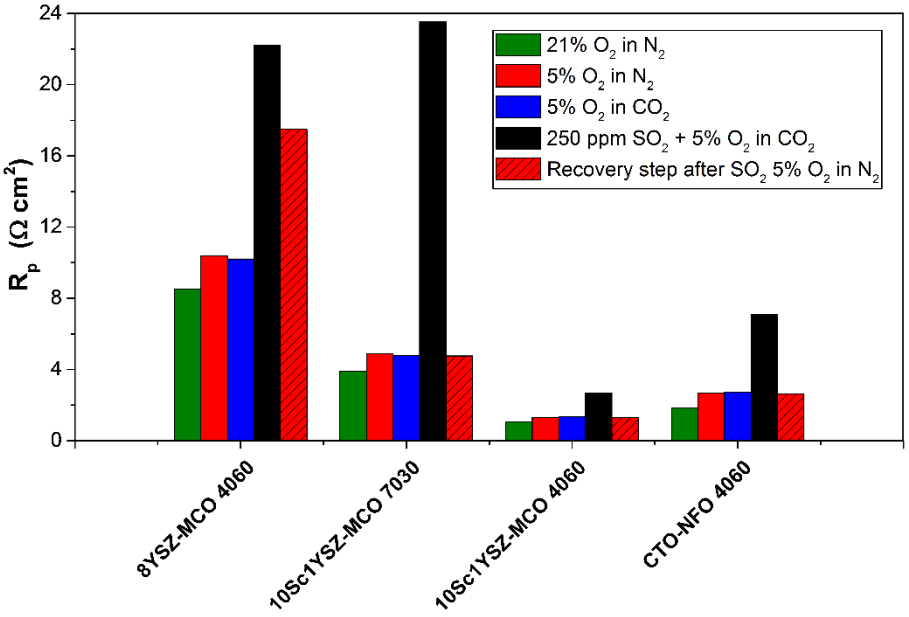

Figure 7: Representation of the polarization resistances associated to 8YSZ-MCO (40-60 vol.%), 10Sc1YSZ-MCO (70-30 vol.%), 10Sc1YSZ-MCO (40-60 vol.%) and CTO-NFO (40-60 vol.%) non-infiltrated porous backbones.

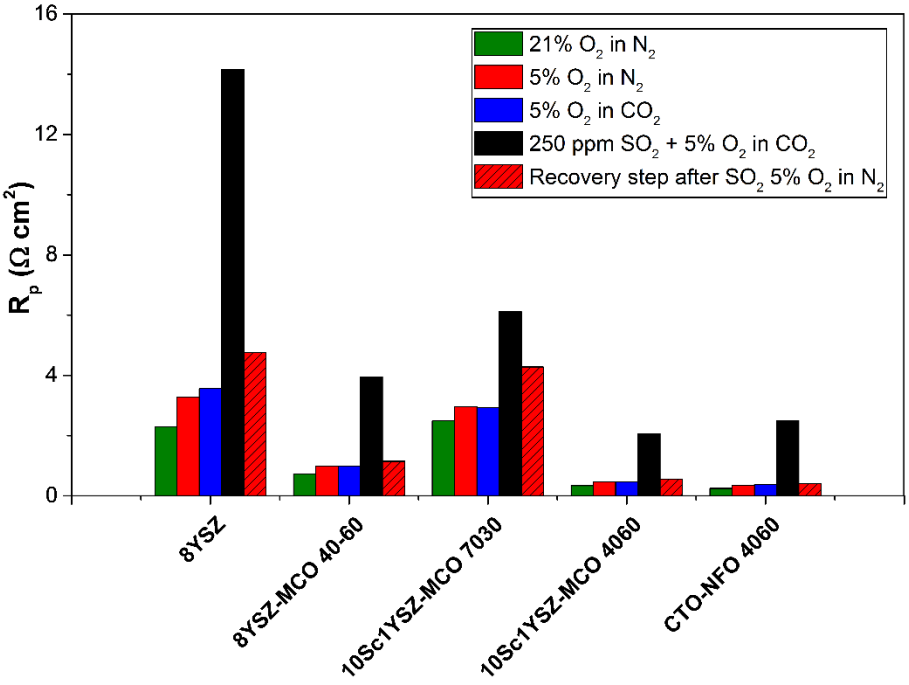

Figure 8: Representation of the polarization resistances associated to 8YSZ, 8YSZ-MCO (40-60 vol.%), 10Sc1YSZ-MCO (70-30 vol.%), 10Sc1YSZ-MCO (40-60 vol.%) and CTO-NFO (40-60 vol.%) porous backbones infiltrated by a Ce-Pr nitrates based catalytic solution.

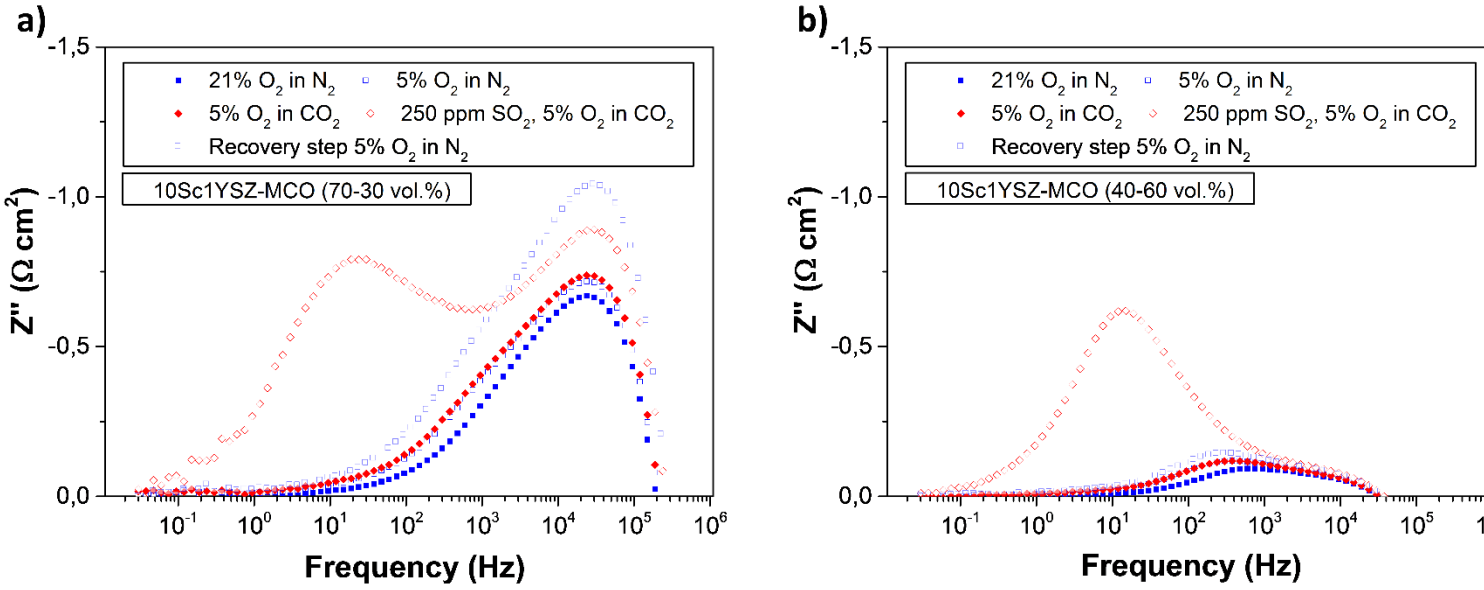

Figure 9: Bode plots for the 10Sc1YSZ-MCO (70-30 vol.%) porous backbone (a) and the 10Sc1YSZ-MCO (40-60 vol.%) porous backbone (b) infiltrated by a Ce-Pr nitrates based catalytic solution. Measurements were performed at 850˚C under different atmospheres.

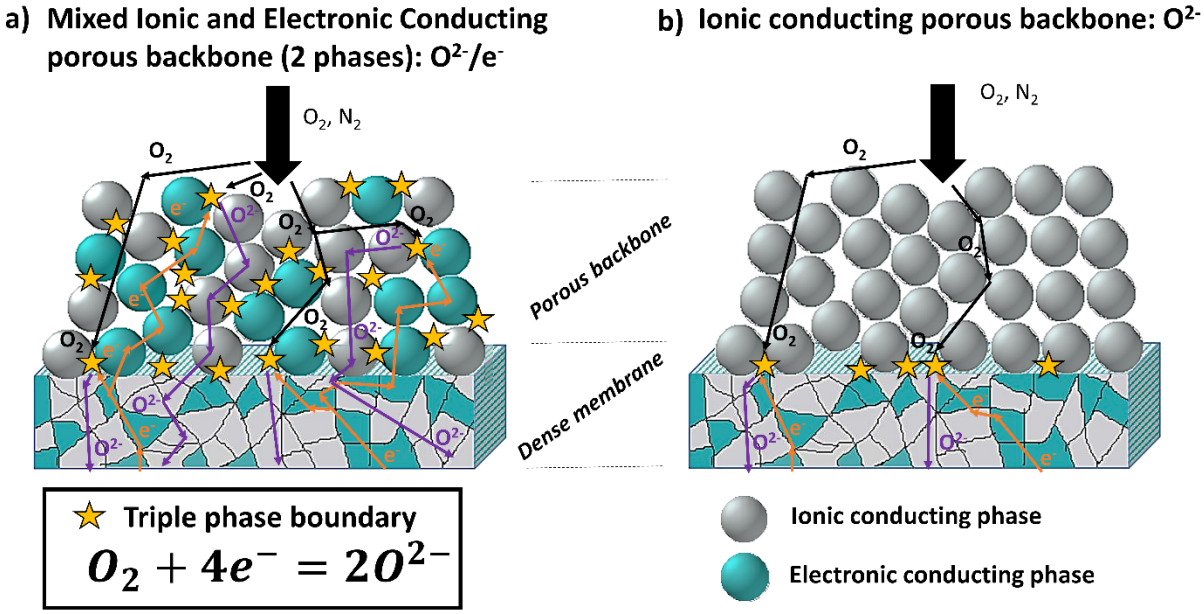

Figure 10: Schematic illustrations of the mechanism of the oxygen reduction reaction considering two cases: (a) a membrane coated with a composite porous backbone formed by a good ionic and a good electronic conductor, and (b) a membrane coated with a purely ionic conducting porous backbone (single-phase).

3.3. Oxygen permeation tests

Figure 11 shows the oxygen permeation flux through 10Sc1YSZ-MCO symmetrical membranes coated with different porous backbones (Figure 11.a: 8YSZ, 11.b: 10Sc1YSZ-MCO (70-30 vol.%) and 11.c: CTO-NFO (40-60 vol.%)) and uncoated (Figure 11.d). The tests were performed at 850 ˚C using different sweep gases. They were sequenced as: (i) test in Ar (150 ml_N min^{-1}, 2 h, black symbols), (ii) test in 70 % Ar + 30 % CO_2 (150 ml_N min^{-1}, 12 h, red symbols), (iii) test in 70 % Ar + 30 % CO_2 + 250 ppm of SO_2 (150 ml_N min^{-1}, 12 h, blue symbols) and (iv) recovery step in Ar (150 ml_N min^{-1}, black symbols). Air was used as a feed gas for the complete duration of the tests and was fed at 100 ml_N min^{-1}.

In clean conditions (sweep gas: Ar, phase (i)) the membrane with CTO-NFO backbones presents the highest oxygen permeation flux (0.28 ml_N min^{-1} cm^{-2}), while the uncoated one displays the lowest performance (0.18 ml_N min^{-1} cm^{-2}). The results observed during phase (i) are in accordance with the results of the EIS measurements: the backbone having the lowest polarization resistance (CTO-NFO) presents the highest oxygen permeation flux. All membranes displayed a stable flux in 30 % CO_2 (phase (ii)). Nevertheless, when the sweep gas was switched from 30 % CO_2 to 250 ppm SO_2 in 70 % Ar + 30 % CO_2, the oxygen permeation fluxes dropped around 0.10 ml_N min^{-1} cm^{-2} no matters the catalytic backbone coated. The loss of permeation can be ascribed to the fact that SO_2 affects the oxygen permeation due to competitive adsorption phenomena on the membrane surfaces [29]. Despite this drop, the oxygen permeation flux is still acceptable when compared with the dramatic oxygen permeation degradations of state-of-the-art oxygen membranes when exposed to sulfur and carbon dioxide containing environments [25][26][38][39]. For example, BSCF membranes show very high oxygen permeability when He is used as a sweep gas (2.76 mL_N cm^{-2} min^{-1} at 900 °C), but the oxygen flux drops near zero when changing the sweep gas to pure CO_2 [25]. Significant degradations of the oxygen permeability were also observed with LSCF membranes exposed to SO_2. Gao et al. reported an oxygen permeability drop of 80 % after exposure to SO_2 [26]. Finally, when returning to clean conditions (phase (iv)), oxygen permeation flux can be recovered reflecting thus the stability of the materials. Only the membrane coated with the CTO-NFO porous catalytic backbones do not

recover the initial oxygen permeability (65 % recovery). This result could be the consequence of a delamination of the porous catalytic backbone due to the different material used in the membrane and in the backbone.

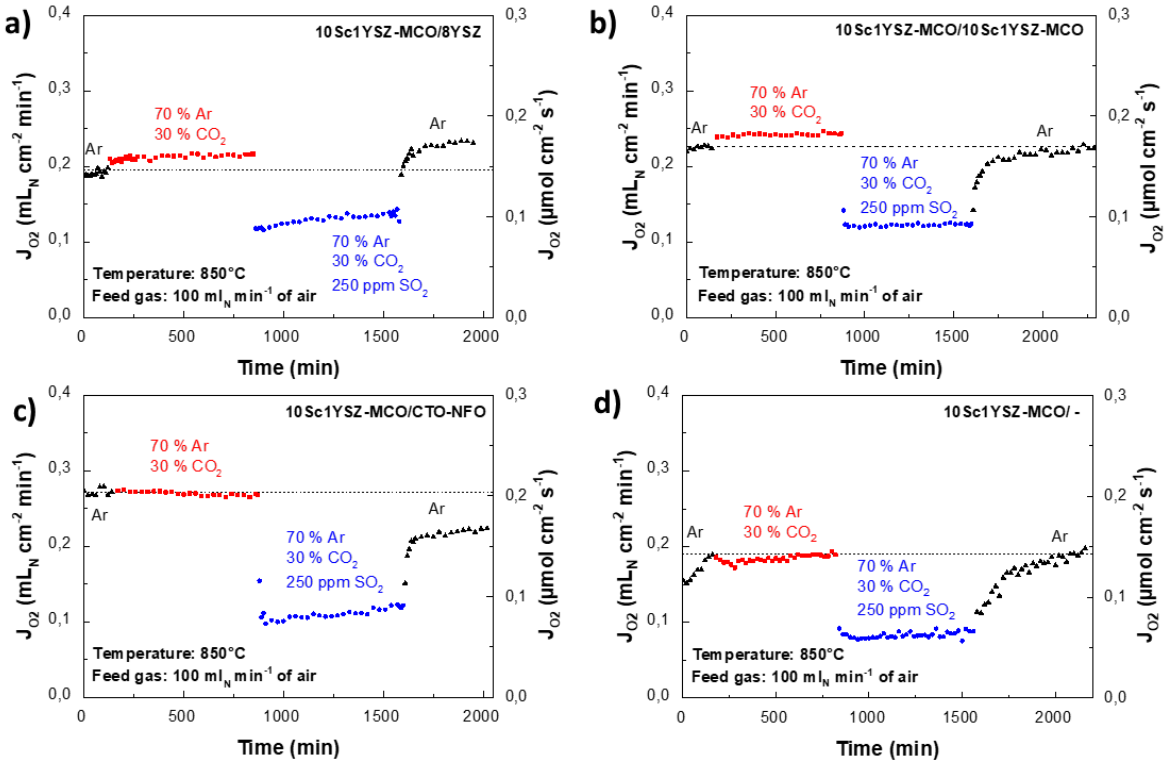

Figure 11: Oxygen permeation flux of 0.5 mm thick 10Sc1YSZ-MCO (70-30 vol.%) membranes as a function of the time. Graphs (a), (b) and (c) display the performances of membranes coated with infiltrated (Ce-Pr catalyst) porous catalytic backbones made of 8YSZ, 10Sc1YSZ-MCO (70-30 vol.%), and CTO-NFO (40-60 vol.%), respectively. The graph (d) shows the performance of an uncoated membrane. The tests were performed in 4 different sweep gas atmosphere: (i) Ar, (ii) 70 % Ar + 30 % CO_2, (iii) 70 % Ar + 30 % CO_2 + 250 ppm SO_2 and (iv) Ar (recovery step).

Conclusion

The stability of a 7 µm thick 10Sc1YSZ-MCO (70-30 vol.%) dual-phase membrane was studied in simulated oxy-fuel combustion conditions (250 ppm SO_2, 3 % H_2O, 5 % O_2 balanced with CO_2). The results of the tests underlined the excellent stability of the membrane in SO_2 and CO_2 containing atmospheres. To achieve a better understanding of the oxygen surface reactions (especially in SO_2 and CO_2 containing atmospheres), electrochemical impedance spectroscopy (EIS) measurements were performed on porous catalytic backbones consisting of: (i) 8YSZ, (ii) 8YSZ-MCO (40-60 vol.%), (iii) 10Sc1YSZ-MCO (40-60 vol.%), (iv) 10Sc1YSZ-MCO (70-30 vol.%), and (v)

$Ce_{0.8}Tb_{0.2}O_{2-\delta}$ (CTO) - $NiFe_2O_4$ (NFO) (40-60 vol.%). The lowest polarization resistances (R_p) were acquired with 10Sc1YSZ-MCO (40-60 vol.%) and CTO-NFO (40-60 vol.%) porous backbones, demonstrating the importance of a mixed ionic and electronic conductivity in the performance of catalytic porous backbones. Oxygen permeation tests were realized on three 10Sc1YSZ-MCO membranes coated with different porous backbones ((i) 8YSZ, (ii) 10Sc1YSZ-MCO (70-30 vol.%) and (iii) CTO-NFO (40-60 vol.%)) which were infiltrated with Ce and Pr nano-particulate catalysts and on an uncoated 10Sc1YSZ-MCO membrane. The CTO-NFO activated backbone increased the oxygen permeation flux about 55 % (0.28 $mL_N\ cm^{-2}\ min^{-1}$, 850 °C, air/Ar) compared to the membrane with no coatings (0.18 $mL_N\ cm^{-2}\ min^{-1}$, 850 °C, air/Ar). A significant influence of SO_2 on the oxygen oxidation/reduction reactions was observed, as R_p and the oxygen permeability of the samples exposed to 250 ppm of SO_2 were significantly affected. Nevertheless, no microstructural degradation was found after SO_2 exposure and initial R_p/oxygen permeation fluxes could be recovered in most of the cases.

[1] H. Stadler, F. Beggel, M. Habermehl, B. Persigehl, R. Kneer, M. Modigell, P. Jeschke, Oxyfuel coal combustion by efficient integration of oxygen transport membranes, Int. J. Greenh. Gas Control. 5 (2011) 7–15. doi:10.1016/j.ijggc.2010.03.004.

[2] H. Stadler, F. Beggel, M. Habermehl, B. Persigehl, R. Kneer, M. Modigell, P. Jeschke, Oxyfuel coal combustion by efficient integration of oxygen transport membranes, Int. J. Greenh. Gas Control. 5 (2011) 7–15. doi:10.1016/j.ijggc.2010.03.004.

[3] S.M. Hashim, A.R. Mohamed, S. Bhatia, Current status of ceramic-based membranes for oxygen separation from air, Adv. Colloid Interface Sci. 160 (2010) 88–100. doi:10.1016/j.cis.2010.07.007.

[4] S. Smart, C.X.C. Lin, L. Ding, K. Thambimuthu, J.C. Diniz da Costa, Ceramic membranes for gas processing in coal gasification, Energy Environ. Sci. 3 (2010) 268–278. doi:10.1039/b924327e.

[5] M. Czyperek, P. Zapp, H.J.M. Bouwmeester, M. Modigell, K. Ebert, I. Voigt, W.A. Meulenberg, L. Singheiser, D. Stöver, Gas separation membranes for zero-emission fossil power plants: MEM-BRAIN, J. Memb. Sci. 359 (2010) 149–159. doi:10.1016/j.memsci.2010.04.012.

[6] S.S. Hashim, A.R. Mohamed, S. Bhatia, Oxygen separation from air using ceramic-based membrane technology for sustainable fuel production and power generation, Renew. Sustain. Energy Rev. 15 (2011) 1284–1293. doi:10.1016/j.rser.2010.10.002.

[7] M. Puig-Arnavat, S. Soprani, M. Søgaard, K. Engelbrecht, J. Ahrenfeldt, U.B. Henriksen, P.V. Hendriksen, Integration of mixed conducting membranes in an oxygen–steam biomass gasification process, RSC Adv. 3 (2013) 20843–20854. doi:10.1039/c3ra44509g.

[8] E.S. Rubin, A.B. Rao, M.B. Berkenpas, Technical Documentation : Oxygen-based Combustion Systems (Oxyfuels) with Carbon Capture and Storage (CCS), 2007.

[9] P. Haworth, S. Smart, J. Glasscock, J.C. Diniz da Costa, High performance yttrium-doped BSCF hollow fibre membranes, Sep. Purif. Technol. 94 (2012) 16–22. doi:10.1016/j.seppur.2012.04.005.

[10] R. Kiebach, K. Engelbrecht, K. Kwok, S. Molin, M. Søgaard, P. Niehoff, F. Schulze-Küppers, R. Kriegel, J. Kluge, P.V. Hendriksen, Joining of ceramic Ba0.5Sr0.5Co0.8Fe0.2O3 membranes for oxygen production to high temperature alloys, J. Memb. Sci. 506 (2016) 11–21. doi:10.1016/j.memsci.2016.01.050.

[11] S. Baumann, J.M. Serra, M.P. Lobera, S. Escolástico, F. Schulze-Küppers, W.A. Meulenberg, Ultrahigh oxygen permeation flux through supported Ba0.5Sr0.5Co0.8Fe0.2O3-δ membranes, J. Memb. Sci. 377 (2011) 198–205. doi:10.1016/j.memsci.2011.04.050.

[12] M. Arnold, H. Wang, A. Feldhoff, Influence of CO2 on the oxygen permeation performance and the microstructure of perovskite-type (Ba0.5Sr0.5)(Co0.8Fe0.2)O3-?? membranes, J. Memb. Sci. 293 (2007) 44–52. doi:10.1016/j.memsci.2007.01.032.

[13] Z. Shao, W. Yang, Y. Cong, H. Dong, J. Tong, G. Xiong, Investigation of the permeation behavior and stability of a Ba0.5Sr0.5Co0.8Fe0.2O(3-δ) oxygen membrane, J. Memb. Sci. 172 (2000) 177–188. doi:10.1016/S0376-7388(00)00337-9.

[14] L. Ge, W. Zhou, R. Ran, S. Liu, Z. Shao, W. Jin, N. Xu, Properties and performance of A-site deficient (Ba0.5Sr0.5)1-xCo0.8Fe0.2O3-δ for oxygen permeating membrane, J. Memb. Sci. 306 (2007) 318–328.

doi:10.1016/j.memsci.2007.09.004.

[15] Z. Taheri, K. Nazari, N. Seyed-Matin, A.A. Safekordi, B. Ghanbari, S. Zarrinpashne, R. Ahmadi, Comparison of oxygen permeation through some perovskite membranes synthesized with EDTNAD, React. Kinet. Mech. Catal. 100 (2010) 459–469. doi:10.1007/s11144-010-0158-2.

[16] F. Schulze-Küppers, S. Baumann, F. Tietz, H.J.M. Bouwmeester, W.A. Meulenberg, Towards the fabrication of La0.98-xSrxCo0.2Fe0.8O3-δ perovskite-type oxygen transport membranes, J. Eur. Ceram. Soc. 34 (2014) 3741–3748. doi:10.1016/j.jeurceramsoc.2014.06.012.

[17] X. Tan, Z. Wang, B. Meng, X. Meng, K. Li, Pilot-scale production of oxygen from air using perovskite hollow fibre membranes, J. Memb. Sci. 352 (2010) 189–196. doi:10.1016/j.memsci.2010.02.015.

[18] J. Gurauskis, Ø.F. Lohne, D.S. Lagergren, E.T. Wefring, K. Wiik, Oxygen permeation in symmetric and asymmetric La0.2Sr0.8Fe0.8Ta0.2O3-?? membranes, J. Eur. Ceram. Soc. 36 (2016) 1427–1434. doi:10.1016/j.jeurceramsoc.2016.01.004.

[19] M.P. Lobera, M. Balaguer, J. García-Fayos, J.M. Serra, Catalytic Oxide-Ion Conducting Materials for Surface Activation of Ba0.5Sr0.5Co0.8Fe0.2O3-d Membranes, ChemistrySelect. 2 (2017) 2949–2955. doi:10.1002/slct.201700530.

[20] E. Bucher, A. Egger, G.B. Caraman, W. Sitte, Stability of the SOFC Cathode Material (Ba,Sr)(Co,Fe)O3−δ in CO2-Containing Atmospheres, J. Electrochem. Soc. 155 (2008) B1218. doi:10.1149/1.2981024.

[21] X. Tan, N. Liu, B. Meng, J. Sunarso, K. Zhang, S. Liu, Oxygen permeation behavior of La0.6Sr0.4Co0.8Fe0.2O3 hollow fibre membranes with highly concentrated CO2 exposure, J. Memb. Sci. 389 (2012) 216–222. doi:10.1016/j.memsci.2011.10.032.

[22] M. Pilar Lobera, S. Escolastico, J. Garcia-Fayos, J.M. Serra, Ethylene Production by ODHE in Catalytically Modified Ba0.5Sr0.5Co0.8Fe0.2O3-delta Membrane Reactors, ChemSusChem. 5 (2012) 1587–1596. doi:10.1002/cssc.201100747.

[23] S.J. Benson, D. Waller, J.A. Kilner, Degradation of La 0.6 Sr 0.4 Fe 0.8 Co 0.2 O 3-d in Carbon Dioxide and Water Atmospheres, J. Electrochem. Soc. 146 (2000) 1305–1309.

[24] M. Schulz, R. Kriegel, A. Kämpfer, Assessment of CO 2 stability and oxygen flux of oxygen permeable membranes, J. Memb. Sci. 378 (2011) 10–17. doi:10.1016/j.memsci.2011.02.037.

[25] S. Engels, T. Markus, M. Modigell, L. Singheiser, Oxygen permeation and stability investigations on MIEC membrane materials under operating conditions for power plant processes, J. Memb. Sci. 370 (2011) 58–69. doi:10.1016/j.memsci.2010.12.021.

[26] J. Gao, L. Li, Z. Yin, J. Zhang, S. Lu, X. Tan, Poisoning effect of SO2 on the oxygen permeation behavior of La0.6Sr0.4Co0.2Fe0.8O3-δ perovskite hollow fiber membranes, J. Memb. Sci. 455 (2014) 341–348. doi:10.1016/j.memsci.2013.12.073.

[27] S. Pirou, J. Gurauskis, V. Gil, M. Søgaard, P.V. Hendriksen, A. Kaiser, S. Ovtar, R. Kiebach, Oxygen permeation flux through 10Sc1YSZ-MnCo2O4 asymmetric membranes prepared by two-step sintering, Fuel Process. Technol. 152 (2016) 192–199. doi:10.1016/j.fuproc.2016.06.019.

[28] A. Samson, M. Søgaard, R. Knibbe, N. Bonanos, High Performance Cathodes for Solid Oxide Fuel Cells

Prepared by Infiltration of La0.6Sr0.4CoO3−δ into Gd-Doped Ceria, J. Electrochem. Soc. 158 (2011) B650. doi:10.1149/1.3571249.

[29] J. Garcia-Fayos, M. Balaguer, J.M. Serra, Dual-Phase Oxygen Transport Membranes for Stable Operation in Environments Containing Carbon Dioxide and Sulfur Dioxide, ChemSusChem. 8 (2015) 4242–4249. doi:10.1002/cssc.201500951.

[30] S. Pirou, J.M. Bermudez, P.V. Hendriksen, A. Kaiser, T. Ramirez, M. Millan, R. Kiebach, Stability and performance of robust dual-phase (ZrO2)0.89(Y2O3)0.01(Sc2O3)0.10-Al0.02Zn0.98O1.01 oxygen transport membranes, J. Memb. Sci. 543 (2017) 18–27. doi:10.1016/j.memsci.2017.08.044.

[31] I. Kuritsyna, V. Sinitsyn, A. Melnikov, Y. Fedotov, E. Tsipis, A. Viskup, S. Bredikhin, V. Kharton, Oxygen exchange, thermochemical expansion and cathodic behavior of perovskite-like Sr0.7Ce0.3MnO3-δ, Solid State Ionics. 262 (2014) 349–353. doi:10.1016/j.ssi.2013.11.013.

[32] T.M. McCoy, Extension of the master sintering curve for constant heating rate modeling, Georgia Institute of Technology, 2008.

[33] X.J. Chen, K.A. Khor, S.H. Chan, L.G. Yu, Influence of microstructure on the ionic conductivity of yttria-stabilized zirconia electrolyte, Mater. Sci. Eng. A. 335 (2002) 246–252. doi:10.1016/S0921-5093(01)01935-9.

[34] J.T.S. Irvine, J.W.L. Dobson, T. Politova, S.G. Martin, A. Shenouda, Co-doping of scandia-zirconia electrolytes for SOFCs., Faraday Discuss. 134 (2007) 41–49; discussion 103–118, 415–419. doi:10.1039/b604441g.

[35] M. Balaguer, C. Solís, J.M. Serra, Study of the transport properties of the mixed ionic electronic conductor Ce1-xTbxO2-δ + Co (x = 0.1, 0.2) and evaluation as oxygen-transport membrane, Chem. Mater. 23 (2011) 2333–2343. doi:10.1021/cm103581w.

[36] A. Petric, H. Ling, Electrical conductivity and thermal expansion of spinels at elevated temperatures, J. Am. Ceram. Soc. 90 (2007) 1515–1520. doi:10.1111/j.1551-2916.2007.01522.x.

[37] L. Navarrete, M. Balaguer, V.B. Vert, J.M. Serra, Tailoring Electrocatalytic Properties of Solid Oxide Fuel Cell Composite Cathodes Based on (La0.8Sr0.2)0.95MnO3+δ and Doped Cerias Ce1-xLnxO2-δ (Ln=Gd, La, Er, Pr, Tb and x=0.1-0.2), Fuel Cells. 17 (2017) 100–107. doi:10.1002/fuce.201600133.

[38] Y. Alqaheem, A. Thursfield, G. Zhang, I.S. Metcalfe, The impact of sulfur contamination on the performance of La 0.6Sr0.4Co0.2Fe0.8O3-d oxygen transport membranes, Solid State Ionics. 262 (2014) 262–265. doi:10.1016/j.ssi.2014.01.011.

[39] A. Waindich, A. Möbius, M. Müller, Corrosion of Ba1-xSrxCo1-yFeyO3-d and La0.3Ba0.7Co0.2Fe0.8O3-d materials for oxygen separating membranes under Oxycoal conditions, J. Memb. Sci. 337 (2009) 182–187. doi:10.1016/j.memsci.2009.03.041.